The Astrophysical Journal, 805:140 (6pp), 2015 June 1 doi:10.1088/0004-637X/805/2/140

EXTINCTION AND NEBULAR LINE PROPERTIES OF A *HERSCHEL*-SELECTED LENSED DUSTY STARBURST AT $z = 1.027$

Nicholas Timmons[1], Asantha Cooray[1], Hooshang Nayyeri[1], Caitlin Casey[1], Jae Calanog[1], Brian Ma[1], Hugo Messias[2], Maarten Baes[3], R. Shane Bussmann[9], Loretta Dunne[4,7], Simon Dye[11], Steve Eales[5], Hai Fu[6], R. J. Ivison[7,8], Steve Maddox[4,7], Michał J. Michałowski[7], I. Oteo[7,8], Dominik A. Riechers[9], Elisabetta Valiante[5], and Julie Wardlow[10]
[1] Department of Physics and Astronomy, University of California, Irvine, CA 92697, USA
[2] Instituto de Astrofísica e Ciências do Espaço, Universidade de Lisboa, OAL, Tapada da Ajuda, PT 1349-018 Lisboa, Portugal
[3] Sterrenkundig Observatorium, UGent, Krijgslaan 281 S9, B-9000 Gent, Belgium
[4] Department of Physics and Astronomy, University of Canterbury, Private Bag 4800, Christchurch, New Zealand
[5] School of Physics and Astronomy, Cardiff University, Queens Buildings, The Parade, Cardiff CF24 3AA, UK
[6] Department of Physics & Astronomy, University of Iowa, Iowa City, IA 52242, USA
[7] Institute for Astronomy, Royal Observatory, Blackford Hill, Edinburgh, EH9 3HJ, UK
[8] European Southern Observatory, Karl-Schwarzschild-Str. 2, D-85748 Garching, Germany
[9] Department of Astronomy, Cornell University, Ithaca, NY 14853, USA
[10] Dark Cosmology Centre, Niels Bohr Institute, University of Copenhagen, Denmark
[11] School of Physics and Astronomy, The University of Nottingham, University Park, Nottingham, NG7 2RD, UK
Received 2015 January 5; accepted 2015 March 28; published 2015 May 28

ABSTRACT

We present *Hubble Space Telescope* Wide Field Camera 3 (WFC3) imaging and grism spectroscopy observations of the *Herschel*-selected gravitationally lensed starburst galaxy HATLASJ1429-0028. The lensing system consists of an edge-on foreground disk galaxy at $z = 0.218$ with a nearly complete Einstein ring of the infrared luminous galaxy at $z = 1.027$. The WFC3 spectroscopy with G102 and G141 grisms, covering the wavelength range of 0.8–1.7 μm, resulted in detections of Hα + [NII], Hβ, [SII], and [OIII] for the background galaxy from which we measure line fluxes and ratios. The Balmer line ratio Hα/Hβ of 7.5 ± 4.4, when corrected for [NII], results in an extinction for the starburst galaxy of $E(B - V) = 0.8 \pm 0.5$. The Hα-based star formation rate (SFR), when corrected for extinction, is $60 \pm 50\, M_{\odot}$ yr^{-1}, lower than the instantaneous SFR of $390 \pm 90\, M_{\odot}$ yr^{-1} from the total IR luminosity. We also compare the nebular line ratios of HATLASJ1429-0028 with other star-forming and sub-millimeter bright galaxies. The nebular line ratios are consistent with an intrinsic ultra-luminous infrared galaxy with no evidence for excitation by an active galactic nucleus (AGN). We estimate the metallicity, 12 + log(O/H), of HATLASJ1429-0028 to be 8.49 ± 0.16. Such a low value is below the average relation for stellar mass versus metallicity of galaxies at $z \sim 1$ for a galaxy with a stellar mass of $\sim 2 \times 10^{11}\, M_{\odot}$. The combination of high stellar mass, the lack of AGN indicators, low metallicity, and the high SFR of HATLASJ1429-0028 suggest that this galaxy is currently undergoing a rapid formation.

Key words: cosmology: observations – galaxies: evolution – infrared: galaxies – submillimeter: galaxies

1. INTRODUCTION

Dusty star-bursting galaxies, especially those that are identified at far-IR/sub-millimeter wavelengths, have infrared luminosities $L_{\rm IR} \sim 10^{12} - 10^{13}\, L_{\odot}$, implying star formation rates (SFRs) in excess of $200\, M_{\odot}$ yr^{-1} (see the review by Casey et al. 2014). As a primary contributor to the cosmic far-IR background, a significant fraction of cosmic star formation and metal production could have occurred in these star-bursting galaxies. Due to deep and wide surveys with the *Herschel Space Observatory* (Pilbratt et al. 2010), we now have large samples of dusty, star-burst galaxies at $z > 1$. Despite large number statistics our knowledge on the physical processes within such galaxies is still limited.

Traditional studies at optical and IR wavelengths involving nebular lines to probe the interstellar medium (ISM) of these dusty starbursts are challenging due to high dust extinction. One way to overcome this limitation is to make use of the flux magnification provided by gravitational lensing. Sub-millimeter surveys provide an efficient way to select lensed high-redshift galaxies due to the negative K-correction of the thermal dust spectral energy distribution (SED) and the steep faint-end slope of the sub-millimeter source counts (Blain 1996). The two large area surveys, *Herschel*-ATLAS (Eales et al. 2010) and HerMES (Oliver et al. 2012), have resulted in sufficiently large samples of lensed galaxies (Negrello et al. 2010; Bussmann et al. 2013; Wardlow et al. 2013) from which we can find interesting targets for detailed follow-up observations.

Here we present results on the rest-frame optical spectroscopy of a lensed starburst galaxy to study its nebular line emission and line ratios. We make use of the *Hubble Space Telescope* Wide Field Camera 3 (*HST*/WFC3) grisms for these observations. To detect both Hα and Hβ over the wavelength covered by WFC3 grisms, we require lensed galaxies to be at $z < 1.6$. One feasible target for WFC3 grism observations from currently known lensed *Herschel* sources is HATLASJ142935.3-002836 (Messias et al. 2014; H1429-0028; G15v2.19 in Calanog et al. 2014). The lensed galaxy was detected in the GAMA-15 field of *Herschel*-ATLAS (Eales et al. 2010) with $S_{160\,\mu{\rm m}} = 1.1 \pm 0.1$ *Jy*. The lensing models of the system using a Keck II/NIRC2 laser guide star adaptive optics image and high-resolution ALMA imaging data are presented in Calanog et al. (2014) and Messias et al. (2014). The system includes a foreground edge-on disk galaxy

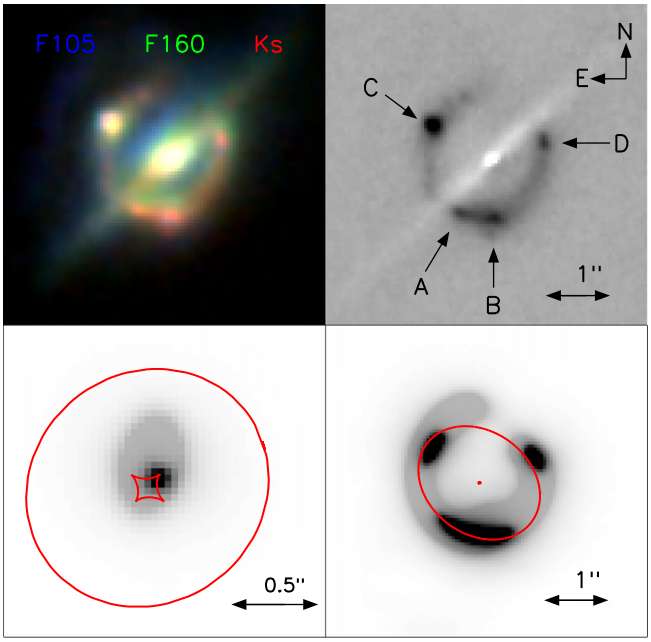

Figure 1. Top left: the three color image of the gravitationally lensed system HATLASJ1429-0028 (also G15v2.19 in Calanog et al. 2014) using WFC3/F105W (blue), F160W (green), and Keck II/NIRC2-LGS K_s (red) imaging data. Top right: the foreground lensing galaxy was modeled using GALFIT (Peng et al. 2002) and then subtracted from the K_s-band imaging data. We label the bright knots following the scheme that was presented in Messias et al. (2014). Bottom left: source plane reconstruction showing the two components of HATLASJ1429-0028 and the caustic curves. Bottom right: image plane reconstruction showing the lens model and the critical curve. Note that the bright features A, B, C, and D are from the bright compact source near the inner cusp caustic while the diffuse ring is due to the extended source.

($z = 0.218$) with a near complete Einstein ring (Figure 1). The lens model in Messias et al. (2014) shows that H1429-0028 is comprised of two components with a mass ratio of $(1 : 2.8^{+1.8}_{-1.5})$. The two components have been used to suggest that H1429-0028 may be undergoing a galaxy merger, but the two components of H1429-0028 are found to lie on top of each other. This also leaves the possibility that the compact bright component of H1429-0028 is a starbursting clump or a region within a galaxy. The full extent of the galaxy is traced by the extended component that is gravitationally lensed to an Einstein ring (Figure 1). The background source is at $z = 1.027$ with a total magnification factor of $\mu = 7.9 \pm 0.8$ at infrared wavelengths (Messias et al. 2014). The K-band (AB) magnitude of H1429-0028 is 18.2 (Calanog et al. 2014) and is at the level that allows grism observations with just one or two *HST* orbits.

Here we report *HST*/WFC3 grism spectroscopic observations of H1429-0028 making use of G102 and G141 grism filters, covering the wavelength range of 0.8–1.7 μm. At the redshift of H1429-0028 these observations probe the rest-frame wavelength range of 0.4–0.8 μm allowing us to measure several photoionization emission lines. We use these measurements to explore the properties of this system in terms of several emission line diagnostic diagrams. We also establish the gas-phase metallicity in a star-forming galaxy. The paper is organized as following: In Section 2 we describe the observations and our data reduction procedure. In Section 3 we present our results related to emission lines and emission line flux ratios and discuss them in the context of existing studies in the literature. We conclude with a summary in

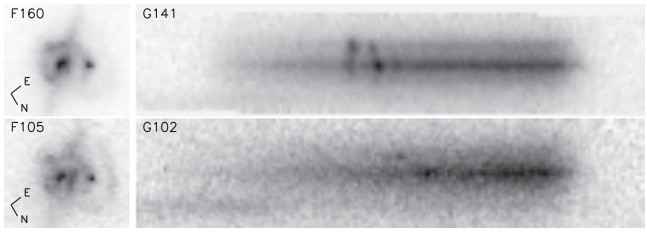

Figure 2. Left: the direct image in each of the WFC3 imaging filters oriented along the dispersion direction of the grism. Right: the two-dimensional grism images of H1429-0028. The top panel shows G141 and F160W images while the bottom panel shows G102 and F105W images. The upper trace contains the signal from knots A + B while the lower trace contains the signal from knot C as well as from the foreground lens.

Section 4. When calculating luminosities we make use of the standard flat-ΛCDM cosmological model with $H_0 = 70\,\mathrm{km\,s^{-1}\,Mpc^{-1}}$ and $\Omega_\Lambda = 0.73$.

2. OBSERVATIONS

HST/WFC3 observations of H1429-0028 were completed with two orbits under GO program 13,399 in Cycle 21 (PI: Cooray). We obtained a total of five exposures, including two direct images and three grism observations in two filters (Figure 2). The two direct images made use of WFC3/F160W and F105W filters for a total of 250 and 350 s, respectively. We obtained G102 and G141 grism observations over 1800 and 2900 s, respectively. The G141 grism covers 1.0–1.8 μm, while the G102 grism covers 0.7–1.2 μm. At $z = 1.027$, these observations allow important emission line studies of H1429-0028 involving Hα at 1.33 μm, Hβ at 0.985 μm, [OIII] at 1.015 and 1.005 μm, and [SII] at 1.364 and 1.361 μm. Due to the low spectral resolution of the order of 80 Å, the data do not resolve the [SII] doublet or Hα from [NII].

We made use of the calibrated *HST* imaging and grism data from the CALWF3 reduction pipeline, as provided by the Space Telescope Science Institute. The spectra for individual objects in the image were extracted with the aXe software package (Kümmel et al. 2009). Briefly, we created an object catalog making use of the broadband F160W and F105W images with the SExtractor package (Bertin & Arnouts 1996). A sky background subtraction was performed on the direct as well as the grism images. The core aXe marks spectral regions for each object in the SExtractor catalog, estimates contamination from nearby sources, and flat fields each of those regions or beams. A two-dimensional stamp of each grism beam is generated and then combined together with multiple observations of the same stamp to create a final two-dimensional image for scientific analysis. The data products include the two-dimensional combined grism stamp for each object as well as flux-calibrated one-dimensional spectra, contamination estimates, and error estimates.

We identified emission lines in the one-dimensional spectra using the known redshift of $z = 1.027$ for H1429-0028. We made use of custom IDL scripts as well as the Pyraf task SPLOT with ICFIT to extract the emission line flux densities and their errors from the one-dimensional spectra. To account for the contamination from the foreground lensing galaxy, we also model a continuum and account for the contamination in our line flux densities. Detailed lens modeling of H1429-0028 in four bands have shown clear evidence for differential magnification. For the rest-frame optical observations as is the

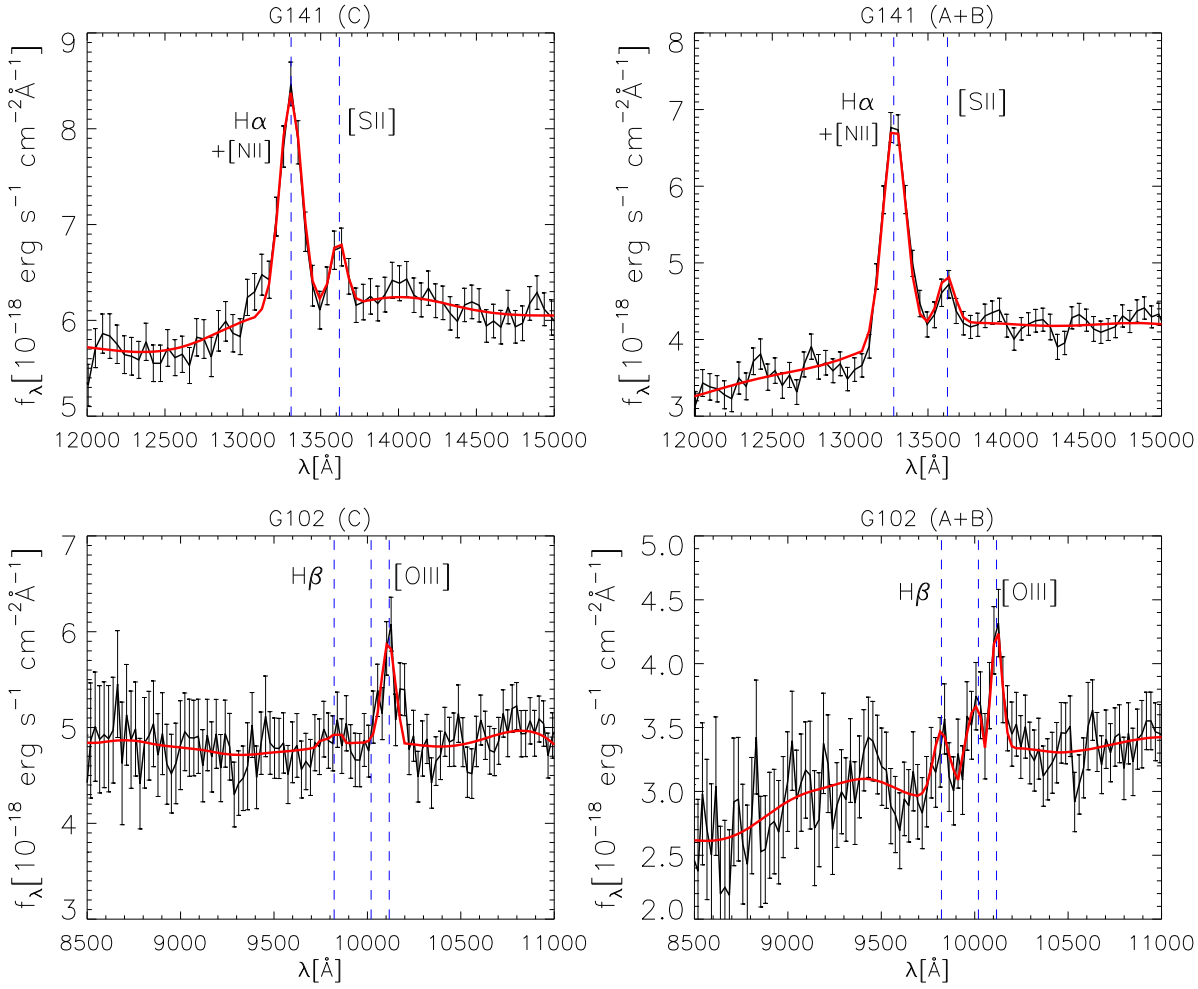

Figure 3. Extracted one-dimensional spectra showing the regions of detected emission lines. We separate these detections into different knots identified in Figure 1, mainly knot C, brightest of the features, and the combination of knots A + B. The spectra from knot C are plotted on the left while the spectra from knots A + B are plotted on the right. Emission lines from knot D were undetected or confused with the continuum emission from the foreground lensing galaxy in the dispersion direction of the two grism observations.

case for our data the appropriate magnification is 7.9 ± 0.8 (Messias et al. 2014).

3. RESULTS

In order to derive extinction corrections and line ratios, we measure the line intensities for detected bright regions of H1429-0028. In Figure 1, we label the bright components following the scheme of Messias et al. (2014). In Figure 3, we plot the one-dimensional spectra showing the detected emission lines. In the G141 grism, the brightest component C and (A + B) as well as parts of the Einstein ring had clear emission detections. For G102, only components (A + B) had detectable [OIII] as well as Hβ. In G102, component C had a clear detection of the [OIII] lines, but only an upper limit on the Hβ line. Table 1 lists the measured line fluxes and equivalent widths for each detection. Given the ratio of Hα to Hβ in knots (A + B), and the detected value of Hα in knot C, the expected value of Hβ in knot C is $\sim 3.2 \pm 1.9 \times 10^{-17}$ erg s^{-1} cm^{-2}. We measured the Hβ line flux density to be $1.4 \pm 3.8 \times 10^{-17}$ erg s^{-1} cm^{-2}. This value falls within the estimated range, but is not robust enough to be used for scientific analysis.

From Figure 1, the lens models suggest two components for H1429-0028, one that is compact and bright and a second that is extended. The two components have effective radii of 0.″18 ± 0.01 and 0.″03 ± 0.01, for the source responsible for the ring and for knots, respectively. It is clear from the lensing models that the quadruply imaged knots A to D are from the same source. While it has been suggested that H1429-0028 is a merger, due to the presence of two components in the lens

Table 1
Emission Lines

Line	Component	Flux[a]	Equation Width[b] (Å)
Hα+[NII]	(A+B)	45.8 ± 2.3	108.4 ± 5.4
Hα+[NII]	(C)	32.9 ± 2.6	52.4 ± 4.2
Hβ	(A+B)	4.5 ± 2.6	15.1 ± 8.8
Hβ	(C)	1.4 ± 3.8	2.9 ± 8.0
[OIII]λ(5007)	(A+B)	6.4 ± 1.8	18.8 ± 5.2
[OIII]λ(4959)	(A+B)	4.1 ± 1.9	12.6 ± 5.9
[OIII]λ(5007+4959)	(C)	10.8 ± 2.2	22.6 ± 4.7
[SII](doublet)	(A+B)	10.1 ± 1.8	23.7 ± 4.2
[SII](doublet)	(C)	8.7 ± 2.1	14.1 ± 3.4

[a] Line fluxes are in 10^{-17} erg s^{-1} cm^{-2}, and are not corrected for lens magnification.
[b] Equivalent widths should be considered as an upper limit due to potential systematic uncertainties in the background continuum model.

model, it is not clear from such a model if H1429-0028 is two separate galaxies or if the smaller component is a high star-forming region within a galaxy. Our spectral line data do not have the adequate velocity resolution, but in the future this question can be addressed with integral field unit observations. In this work, for the line ratios, we only study the ratios of bright knots. Thus our line ratios capture the physical properties within the starbursting compact region or a compact galaxy. For the total Hα flux, we add the flux from each component with their corresponding magnification from the lens model. The values are a magnification factor of $\mu \sim 27$ for the compact component, which contributes to the bright knots, and $\mu \sim 10$ for the larger component which contributes to the ring. We scale the observed line flux to a total estimate of the line intensity across the galaxy based on K-band photometry of the bright components and the diffuse rings. This correction results in a factor of 2.6 ± 0.1 from the line fluxes measured for the sum of the components A + B + C to the galaxy as a whole assuming that the continuum fluxes detected for the other components and ring scale as the rest-frame optical magnitudes.

To correct for the [NII] contamination of Hα we make use of two independent methods to derive the expected [NII]/Hα line ratio and average them as the final value to use here. This follows the approach given in Domínguez et al. (2013). The first method from Sobral et al. (2012) estimates the [NII]/Hα ratio using the Hα + [NII] equivalent widths (EWs). Using the measured EWs, we estimate the ratio to be 0.27 ± 0.07. However, it could be that we are overestimating the EWs in our line fitting procedure due to systematic uncertainties associated with the model for the continuum, especially since the continuum is dominated by the residual fluxes from the foreground lensing galaxy. Thus we also employ a second method, but we find consistent estimates on the [NII]/Hα ratio.

The second method from Erb et al. (2006) relies on a relationship derived between the stellar mass of a galaxy and the Hα/NII ratio of that galaxy. Here, instead of an independent estimate of the stellar mass, we make use of the SED modeling in Ma et al. (2015) with a stellar mass of $1.9 \pm 0.02 \times 10^{11}\,M_{\odot}$ derived from MAGPHYS. The resulting [NII]/Hα ratio is 0.27 ± 0.03. Both Sobral et al. (2012) and Erb et al. (2006) make use of the calibration method used in Pettini & Pagel (2004). The two estimates are consistent with each other. Note that the stellar mass we use is slightly lower than the value of $\sim 3 \times 10^{11}\,M_{\odot}$ quoted by Messias et al. (2014). We prefer to use a revised value for the stellar mass using MAGPHYS models as we include new optical measurements of the SED and, as discussed later, we find consistent estimates on the extinction with SED modeling when compared to the estimates based on the Balmer line ratios.

For the values we discuss below, we take the average ratio of [NII]/Hα from Sobral et al. (2012) and Erb et al. (2006) to be 0.27 ± 0.05. Once corrected for [NII], we find Hα/H$\beta = 7.49 \pm 4.4$. Using this ratio, we calculate the nebular extinction $E(B-V)$ following Momcheva et al. (2013) and find it to be 0.82 ± 0.50. Using Calzetti (2001), the corresponding optical depth τ_V is 2.93 ± 1.9. The extinction is lower than the τ_V value of $\sim 11.2^{+4.5}_{-3.2}$ for H1429-0028 in Messias et al. (2014), based on the broad-based SED model fitting using MAGPHYS. A revised model fit to H1429-0028 using new estimates of the background galaxy, including deblended IRAC data, finds $\tau_V \sim 4.2 \pm 0.4$ consistent with the estimate of τ_V from the Balmer line ratios (Ma et al. 2015, in preparation).

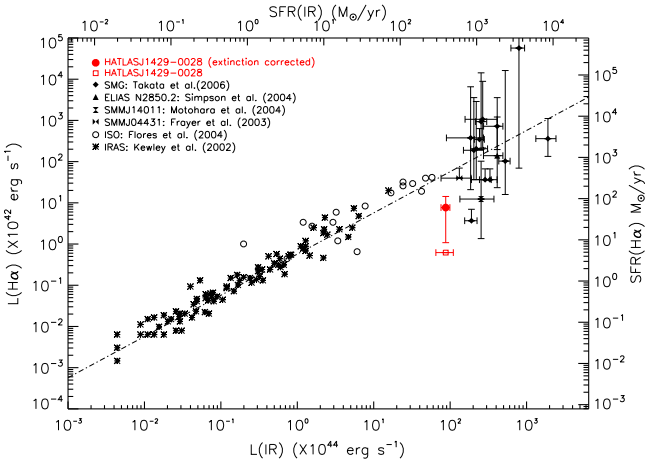

Figure 4. Hα luminosity vs. far-infrared for H1429-0028 compared to the extinction corrected sample of IR luminous and sub-millimeter galaxies in Takata et al. (2006). For reference, we also show the corresponding SFRs based on IR luminosity and Hα luminosity to the top and left of the plot, respectively. We show H1429-0028 for two cases with and without extinction correction of Hα luminosity. The dotted–dashed line represents the case that SFRs from Hα and far-infrared are equal. H1429-0028 falls below this trend line, but the difference between IR- and Hα-based SFRs is fully consistent with the observed scatter of previous measurements.

In Figure 4, we compare the extinction-corrected Hα luminosity of H1429-0028 with other star-forming galaxies. All data points from the literature (following Takata et al. 2006) are extinction corrected, though we show the case for H1429-0028 with and without extinction correction. Though the apparent luminosity of H1429-0028 corresponds to that of a hyperluminous infrared galaxy with $L_{\rm IR} \sim 10^{13}\ L_{\odot}$, the intrinsic luminosity, once corrected for lensing magnification, is that of an ultraluminous infrared galaxy (ULIRG). The galaxy falls between the SMGs and local ULIRGs studied by Swinbank et al. (2004) and Takata et al. (2006) with rest-frame optical spectroscopy at Keck and Subaru, respectively. We find the extinction-corrected SFR of H1429-0028, at $60 \pm 50\,M_{\odot}\ {\rm yr}^{-1}$, to be lower than the instantaneous SFR implied by the total IR luminosity, with a value of $390 \pm 90\,M_{\odot}\ {\rm yr}^{-1}$ using the Kennicutt (1998) relation. Given the scatter observed in Figure 4, however, we do not find this difference to be statistically significant.

In Figure 5, we compare the Balmer decrement of H1429-0028 against Hα, IR luminosity, and stellar mass for a sample of galaxies. As shown in Figure 5, middle panel, for the sample of galaxies with both Hβ and Hα measurements in the literature, we find the extinction-corrected Hα luminosity of H1429-0028 to be among the highest. The Domínguez et al. (2013) sample comes from *HST*/WFC3 grism observations of $z \sim 0.75$–1.5 galaxies. The SDSS-detected star-forming galaxies have $L_{\rm H\alpha} < 10^{42}$ ergs s^{-1}, while for H1429-0028 $L_{\rm H\alpha} > 10^{43}$ ergs s^{-1}. This is consistent with the fact that H1429-0028 is a ULIRG. The right panel shows the trend in the Balmer decrement with the stellar mass such that there is a slight decrease in the Hβ to Hα ratio with an increase in the stellar mass. The plotted points are the sample-averaged values from Domínguez et al. (2013) as diamonds and Sobral et al. (2012) as squares in three stellar mass bins in both studies. These data mainly probe the stellar mass below a few times

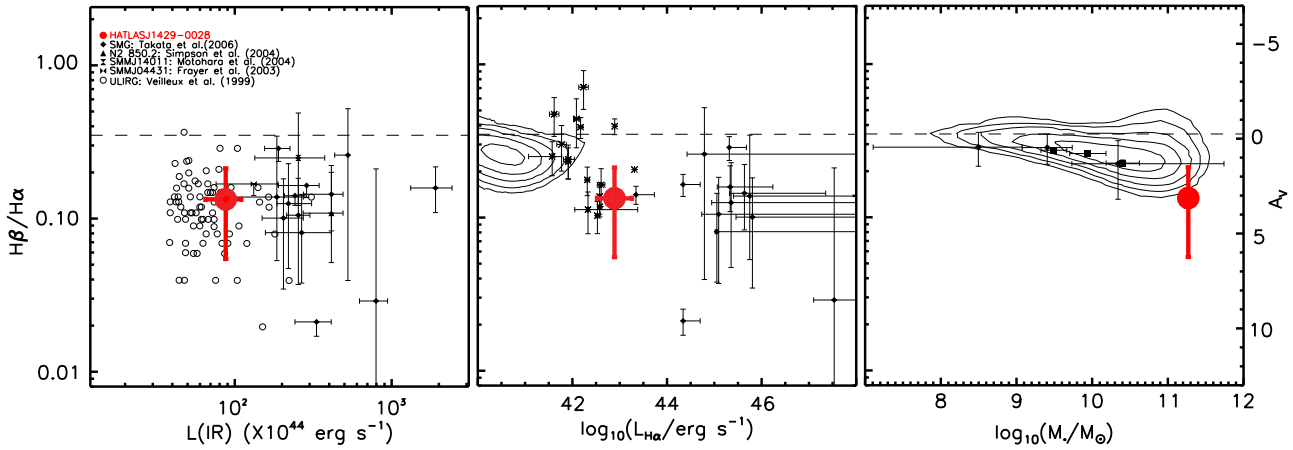

Figure 5. Left: Balmer decrement vs. IR luminosity. The background data are from Takata et al. (2006). Middle: Balmer decrement vs. Hα luminosity. The stars come from Domínguez et al. (2013) and the diamonds are from Takata et al. (2006). The contours show the galaxy population traced by SDSS. Right: Balmer decrement vs. galaxy stellar mass. The contours show the galaxy population traced by SDSS. The diamonds correspond to star-forming galaxies of $0.75 \leqslant z \leqslant 1.5$ presented in Domínguez et al. (2013), while the squares correspond to $z \sim 2$ from Sobral et al. (2012). We show the expected optical attenuation A_V to the right of the right panel for corresponding values of H_β/H_α. The dashed line represents the intrinsic value of the Balmer decrement.

$10^{10}\,M_\odot$. H1429-0028 is massive with $M_\star \sim 10^{11}\ M_\odot$ and has a Balmer decrement that is lower than the typical star-forming galaxies in the same redshift range of 0.75–1.5.

In Figure 6, we compare the line ratios of [OIII]/Hβ versus [SII]/Hα. This is a variant of the more traditional BPT diagram (Baldwin et al. 1981) that involves [OIII]/Hβ versus [NII]/Hα. Given that [NII] is blended with Hα in our low-resolution data, we make use of the [SII]/Hα ratio. We make extinction corrections for the [SII]/Hα ratio here given the two [SII] lines are somewhat separated in wavelength from Hα. In this diagram, H1429-0028 is consistent with the low metallicity end of the star-forming regions, though the ratios have large uncertainties associated with measurement errors. The measurements are incompatible with AGN regions of galaxies from SDSS data at $z < 0.3$. While H1429-0028 is luminous, this is primarily due to gravitational lensing; the intrinsic luminosity of H1429-0028 is compatible with a galaxy star forming at a rate of 200–400 $M_\odot$ yr^{-1}. The lens models shown in Messias et al. (2014) are compatible with a merger system. Interestingly, a value for [NII]/Hα of 0.27 ± 0.03 is higher than the average [NII]/Hα ratio of 0.19 ± 0.05 for the galaxies classified as star-forming in the SCUBA sample of Swinbank et al. (2004), and lower than the average for SMGs hosting AGNs of 0.41 ± 0.05 from the same study.

In Figure 7, we make use of the nebular line ratios, with the estimate of [NII]/Hα ratio, to make an estimate of the metallicity. Instead of an estimate based on the [NII]/Hα ratio alone, we make use of the O3N2 ratio (Pettini & Pagel 2004) as the estimator here because it also involves the measured [OIII]/Hβ ratio. The metallicity value, as measured in terms of 12 + log(O/H), was found to be 8.49 ± 0.16. In Figure 7, we compare the metallicity versus the stellar mass. The figure shows the average metallicity versus stellar mass relations for both local (Mannucci et al. 2010) and $z \sim 2$ galaxies (Steidel et al. 2014). H1429-0028 has a metallicity comparable to galaxies at $z \sim 2$ despite being at $z = 1.027$. H1429-0028 has a high SFR, but shows no indication that it is hosting an AGN. H1429-0028 is metal-poor despite its high stellar mass and argues for a scenario that it is still under a rapid formation phase.

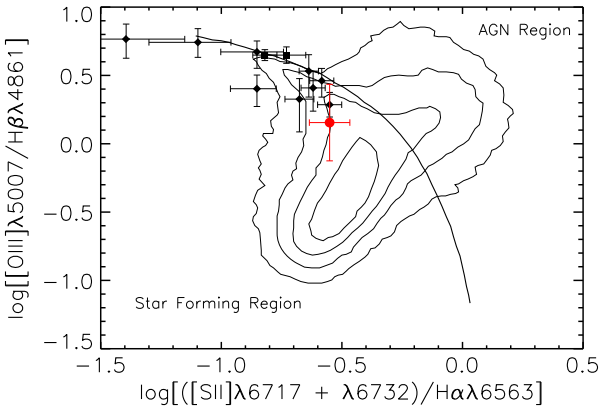

Figure 6. Top: BPT diagram with the black line separating the AGN and star-forming regions Kewley et al. (2001). The red point corresponds to H1429-0028, while the black points come from star-forming galaxies in the redshift range $0.75 \leqslant z \leqslant 1.5$ from Domínguez et al. (2013) represented as diamonds and two $z \sim 2$ lensed star-forming galaxies from Hainline et al. (2009) represented as squares. The background contours show the galaxy population traced by SDSS Kewley et al. (2001).

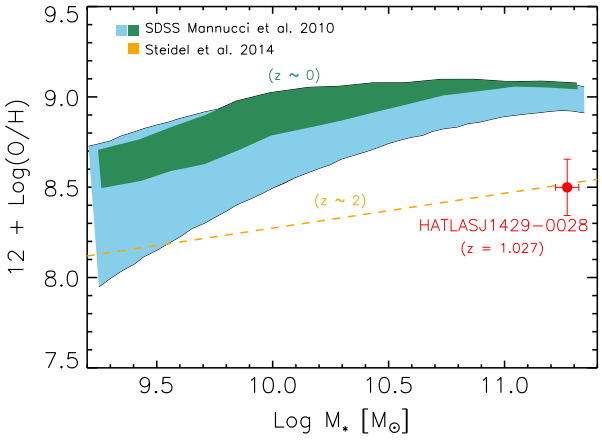

Figure 7. Metallicity vs. Stellar Mass. The green band represents local SDSS galaxies while the blue region represents a second order fit to SDSS extrapolated toward higher SFR (Mannucci et al. 2010). The orange dashed line representing $z \sim 2$ galaxies from Steidel et al. (2014). The calculated value of metallicity for H1429-0028 representing the O3N2 calculation using the O [III]/Hβ to N[II]/Hα ratio (Pettini & Pagel 2004).

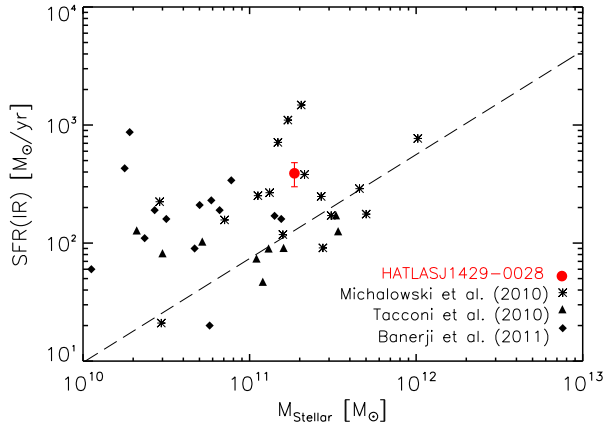

Figure 8. Star formation rate (based on the IR luminosity) vs. stellar mass. For comparison $z \sim 1$ SMGs from Michałowski et al. (2010), Tacconi et al. (2010), and Banerji et al. (2011) are shown. The dashed line shows the $z = 1$ main sequence relation (Elbaz et al. 2007).

Finally, in Figure 8, we show the location of H1429-0028 in comparison to the main sequence of galaxies at $z \sim 1$. Here we plot the total IR luminosity-based SFR of H1429-0028 versus stellar mass. We find that H1429-0028 is above the $z = 1$ correlation from Elbaz et al. (2007). For comparison, we also show other dusty star-forming galaxies at $z \sim 1$ from the literature. Finally the average gas fraction $M_{\rm ISM}/(M_\odot + M_{\rm ISM})$ for the Tacconi et al. (2010) sample of star-forming galaxies is 0.34%. The gas fraction for H1429-0028 is $0.25 \pm 0.1\%$, where we make use of the gas mass of $M_{\rm ISM} = 4.6 \pm 1.7 \times 10^{10}\,M_\odot$ from ALMA CO observations reported in Messias et al. (2014).

H1429-0028 is one example of a grism observation with *HST* based on a galaxy that was first selected with the *Herschel* catalog as a lensed background source. Based on lensing models (Wardlow et al. 2013), we find that there should be roughly 0.25 deg^{-2} lensed starburst galaxies in the redshift interval of one to two. In the future, such galaxies will be automatically included as part of the surveys that will be done with slitless grisms on Euclid and WFIRST. In the 2000 deg^2 High Latitude Deep survey, we expect that WFIRST will detect close to 500 lensed starbursts at $z \sim 1$ to 3. The study we have presented for one lensed galaxy can then be expanded to a large enough sample for detailed statistical study that probes the internal structure of lensed starbursts.

4. SUMMARY

We observed the *Herschel*-selected gravitationally lensed starburst galaxy HATLASJ1429-0028, studied in detail in Messias et al. (2014) with some initial description in Calanog et al. (2014). We present *HST*/WFC3 G101 and G412 grisms of HATLASJ1429-0028. The observations covered the wavelength regime of 0.8–1.7 μm and resulted in detections of Hα + [NII], Hβ, [SII], and [OIII] for several bright regions of the background galaxy. The Balmer line ratio Hα/Hβ of 7.5 ± 4.4, when corrected for [NII], results in an extinction for the starburst galaxy of $E(B-V) = 0.8 \pm 0.5$. The Hα based SFR, when corrected for extinction, is at the level of 60 ± 50 $M_\odot$ yr^{-1}, lower than the star formation rate of $390 \pm 90\,M_\odot$ yr^{-1} from the total IR luminosity. HATLASJ1429-0028 also has a low metallicity despite its high stellar mass at the level of 10^{11} $M_\odot$. The combination of high stellar mass, lack of AGN indicators, low metallicity, and the high SFR of HATLASJ1429-0028 suggests that this galaxy is still going through a rapid formation.

Financial support for this work was provided by NASA through grant *HST*-GO-13399 from the Space Telescope Science Institute, which is operated by Associated Universities for Research in Astronomy, Inc., under NASA contract NAS 5-26555. Additional support for N.T., A.C., H.N., B.M., and C.M.C. was from NSF with AST-1313319. The Dark Cosmology Centre is funded by the Danish National Research Foundation. L.D., R.J.I. and S.J.M. acknowledge support from the European Research Council Advanced grant COSMICISM.

REFERENCES

Baldwin, J. A., Phillips, M. M., & Terlevich, R. 1981, PASP, 93, 5
Banerji, M., Chapman, S. C., Smail, I., et al. 2011, MNRAS, 418, 1071
Bertin, E., & Arnouts, S. 1996, A&AS, 117, 393
Blain, A. W. 1996, MNRAS, 283, 1340
Bussmann, R. S., Pérez-Fournon, I., Amber, S., et al. 2013, ApJ, 779, 25
Calanog, J. A., Fu, H., Cooray, A., et al. 2014, arXiv:1406.1487
Calzetti, D. 2001, PASP, 113, 1449
Casey, C. M., Narayanan, D., & Cooray, A. 2014, PhR, 541, 45
Domínguez, A., Siana, B., Henry, A. L., et al. 2013, ApJ, 763, 145
Eales, S., Dunne, L., Clements, D., et al. 2010, PASP, 122, 499
Elbaz, D., Daddi, E., Le Borgne, D., et al. 2007, A&A, 468, 33
Erb, D. K., Shapley, A. E., Pettini, M., et al. 2006, ApJ, 644, 813
Hainline, K. N., Shapley, A. E., Kornei, K. A., et al. 2009, ApJ, 701, 52
Kennicutt, R. C., Jr. 1998, ARA&A, 36, 189
Kewley, L. J., Dopita, M. A., Sutherland, R. S., Heisler, C. A., & Trevena, J. 2001, ApJ, 556, 121
Kümmel, M., Walsh, J. R., Pirzkal, N., Kuntschner, H., & Pasquali, A. 2009, PASP, 121, 59
Ma, B., Cooray, A., Calanog, J. A., et al. 2015, arXiv:1504.05254
Mannucci, F., Cresci, G., Maiolino, R., Marconi, A., & Gnerucci, A. 2010, MNRAS, 408, 2115
Messias, H., Dye, S., Nagar, N., et al. 2014, A&A, 568, A92
Michałowski, M., Hjorth, J., & Watson, D. 2010, A&A, 514, A67
Momcheva, I. G., Lee, J. C., Ly, C., et al. 2013, AJ, 145, 47
Negrello, M., Hopwood, R., De Zotti, G., et al. 2010, Sci, 330, 800
Oliver, S. J., Bock, J., Altieri, B., et al. 2012, MNRAS, 424, 1614
Peng, C. Y., Ho, L. C., Impey, C. D., & Rix, H.-W. 2002, AJ, 124, 266
Pettini, M., & Pagel, B. E. J. 2004, MNRAS, 348, L59
Pilbratt, G. L., Riedinger, J. R., Passvogel, T., et al. 2010, A&A, 518, L1
Sobral, D., Best, P. N., Matsuda, Y., et al. 2012, MNRAS, 420, 1926
Steidel, C. C., Rudie, G. C., Strom, A. L., et al. 2014, ApJ, 795, 165
Swinbank, M., Smail, I., Chapman, S., et al. 2004, arXiv:astro-ph/0412050
Tacconi, L. J., Genzel, R., Neri, R., et al. 2010, Natur, 463, 781
Takata, T., Sekiguchi, K., Smail, I., et al. 2006, ApJ, 651, 713
Wardlow, J. L., Cooray, A., De Bernardis, F., et al. 2013, ApJ, 762, 59